

Lawrence Berkeley National Laboratory

LBL Publications

Title

Accelerated Zymonic Acid Formation from Pyruvic Acid at the Interface of Aqueous Nanodroplets

Permalink

<https://escholarship.org/uc/item/2jz5s6n9>

Journal

The Journal of Physical Chemistry Letters, 15(44)

ISSN

1948-7185

Authors

Kim, Pyeongeun
Reynolds, Ryan S
Deal, Alexandra M
et al.

Publication Date

2024-11-07

DOI

10.1021/acs.jpcllett.4c02736

Copyright Information

This work is made available under the terms of a Creative Commons Attribution-NonCommercial License, available at <https://creativecommons.org/licenses/by-nc/4.0/>

Peer reviewed

Accelerated Zymonic Acid Formation from Pyruvic Acid at the Interface of Aqueous Nanodroplets

Pyeonggeun Kim, Ryan S. Reynolds, Alexandra M. Deal, Veronica Vaida, Musahid Ahmed, and Kevin R. Wilson*



Cite This: *J. Phys. Chem. Lett.* 2024, 15, 11131–11138



Read Online

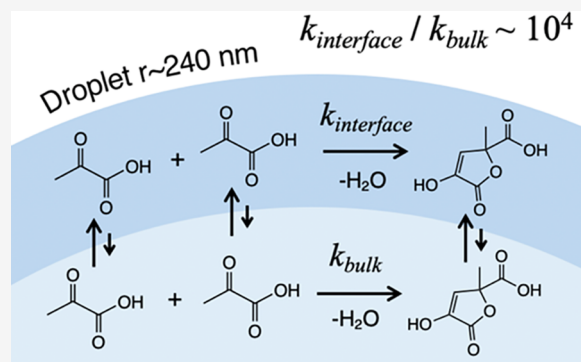
ACCESS |

Metrics & More

Article Recommendations

Supporting Information

ABSTRACT: To explore the role of the liquid interface in mediating reactivity in small compartments, the formation kinetics of zymonic acid (ZA) is measured in submicron aerosols (average radius = 240 nm) using mass spectrometry. The formation of ZA, from a condensation reaction of two pyruvic acid (PA) molecules, proceeds over days in bulk solutions, while in submicron aerosols, it occurs in minutes. The experimental results are replicated in a kinetic model using an apparent interfacial reaction rate coefficient of $k_{rxn} = (0.9 \pm 0.2) \times 10^{-3} \text{ M}^{-1} \text{ s}^{-1}$. The simulation reveals that surface activity of PA coupled with an enhanced interfacial reaction rate drives accelerated ZA formation in aerosols. Experimental and simulated results provide compelling evidence that the condensation reaction of PA occurs exclusively at the aerosol interface with a reaction rate coefficient that is enhanced by 4 orders of magnitude ($\sim 10^4$) relative to what is estimated for macroscale solutions.



Liquid interfaces play a fundamental role in chemical, biological, and environmental processes.^{1–4} Chemical reactions at liquid–liquid and liquid–air interfaces have gained considerable interest over the past decade because of reports of reactions that are accelerated by orders of magnitude compared to those in bulk solutions.^{5–8} Recent studies of enhanced reaction rates in microcompartments (e.g., microdroplets and emulsions) suggest that partial or preferential solvation of reactants at the liquid interface and the large surface to volume ratio are key contributors to reaction acceleration.^{9–15} In the case of condensation reactions, the kinetic and thermodynamic limitations in bulk solutions due to water elimination have been shown to be reduced at the liquid interfaces.^{16,17} Nonetheless, the understanding of reaction acceleration at liquid interfaces and an accurate kinetic description of the interfacial chemistry remain unclear due to the difficulties of quantifying chemical evolution of (sub)-micron-sized systems.

Pyruvic acid (PA) is widely studied α -keto acid. It is abundant in the atmosphere, and contributes to secondary organic aerosol formation by photochemistry.^{18–20} The overlap of solar radiation and the $n-\pi^*$ transition of PA (300–380 nm) has led to extensive studies of PA photochemistry.^{21–26} Interestingly, photochemical reactions of PA at the air–water interface are shown to enhance oligomerization over that observed in the bulk solutions.²⁶ Furthermore, the formation of zymonic acid (ZA, molecular weight = 158 g/mol) from condensation of two PA molecules is observed even in the absence of photochemistry.^{26,27} This result is surprising

as the bulk reaction requires a highly acidic environment (pH ~ 0) to form ZA with a reaction time scale of several weeks to months.^{28,29} Recently, Li et al. showed impressive evidence that this dark condensation reaction occurs in microdroplets deposited on a surface, where ZA formation is rapid (minutes to hours depending on droplet size)^{30,31} and $\sim 10^3$ to 10^4 faster than the bulk solution.³¹ They showed that the formation kinetics of ZA occurs at the interface is autocatalytic and coupled with gas-phase partitioning.^{30,31}

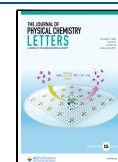
However, questions remain about the kinetics and mechanism of PA chemistry occurring exclusively at the interface of the microdroplets. For example, does the apparent enhanced reaction arise from the interfacial enrichment of reagents or a much larger rate coefficient for the surface reaction? Does ZA produced at the surface stay at the surface or partition to the bulk? To answer these questions, the rate coefficient for ZA formation must be quantified within a realistic kinetic description of the bulk–surface partitioning of PA and ZA.^{26,27,30} Furthermore, since PA is relatively volatile (vapor pressure at 298 K = 175 Pa),^{32,33} the mechanism must

Received: September 18, 2024

Revised: October 22, 2024

Accepted: October 24, 2024

Published: October 31, 2024



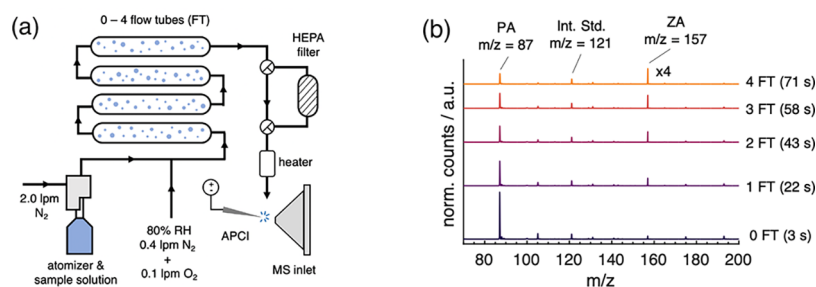


Figure 1. (a) Schematic of the instrumental design for time-resolved mass spectrometric measurements of submicron aqueous aerosols containing PA as a reactant and ZA as a product. APCI denotes atmospheric pressure chemical ionization. RH stands for relative humidity. (b) Time-resolved mass spectra of aerosols generated from aqueous 1 M NaCl and 80 mM PA solution (aerosol $[\text{NaCl}] = 4.6 \text{ M}$ and $[\text{PA}]_0 = 370 \text{ mM}$). Varying the number of flow tubes (FTs) enables measurements of $[\text{PA}]$ and $[\text{ZA}]$ kinetics in aerosols. Succinic acid- d_4 is used as an internal standard (noted as Int. Std. in the spectra).

fully account for the natural competition between desorption and the reaction of PA.

In this study, interfacial reaction kinetics of PA are investigated by measuring the temporal evolution of $[\text{PA}]$ and $[\text{ZA}]$ in aqueous aerosols and analyzing the experimental data using a kinetic model that explicitly accounts for surface and bulk reactions.^{11,34–39} These experiments are aimed at investigating the reactivity of PA in nanosized aerosols using mass spectrometry. By carefully controlling the droplet size and using authentic standards, we analyze the data quantitatively by using a kinetic model. This analysis, which explicitly accounts for surface partitioning of PA and ZA, allows us to quantify how the interfacial reaction rate constant differs from its estimated bulk value. Submicron aerosols of aqueous PA with NaCl ($r_{\text{avg}} = 240 \text{ nm}$, Figure S1) are generated using an atomizer and then directed through a variable number of quartz flow tubes in order to change the reaction time from 3 to 70 s as shown in Figure 1a. NaCl is added to the aerosols to keep the droplet volume constant over the reaction time (i.e., to control the water activity). The atomized droplets are expected to be mildly charged (10s of elementary charge) due to the ionic imbalance occurring during droplet formation.⁴⁰ The impact of the charge on the reaction kinetics is assumed to be minimal. The bulk pH of the solutions from which the droplets are formed ranges from 1.6 for $[\text{PA}]_0 = 370 \text{ mM}$ to 2.0 for $[\text{PA}]_0 = 92 \text{ mM}$. The concentrations of PA and ZA in aerosols are quantified with respect to an internal standard (succinic acid- d_4) with low volatility⁴¹ as a function of time by using aerosol atmospheric pressure chemical ionization mass spectrometry (APCI-MS). Time-resolved aerosol mass spectra are shown in Figure 1b. Experimental design and MS analysis are discussed in detail in the Supporting Information (Figures S1–S3). These aerosol measurements are compared with bulk reactions to ensure that the observed kinetics of PA and ZA occur exclusively in aerosols. A kinetic model is then developed that includes realistic descriptions of bulk-to-interface partitioning, adsorption–desorption at the interface, and interfacial reaction.^{18,32,33,42,43}

The kinetics of $[\text{PA}]$ and $[\text{ZA}]$ in aerosols ($[\text{PA}]_0 = 370 \text{ mM}$) are shown in Figure 2. The simultaneous decrease of $[\text{PA}]$ and formation of $[\text{ZA}]$ is observed. After 70 s, the $[\text{PA}]$ decreased by $\sim 80\%$ (Figure 2a), and $\sim 8 \text{ mM}$ of ZA is detected (Figure 2b). This kinetic behavior is consistent for $[\text{PA}]_0 = 230$ and 90 mM aerosols (Figure S4). To investigate the difference of reaction kinetics in aerosols versus bulk solutions, MS measurements are made from bulk solutions with the same

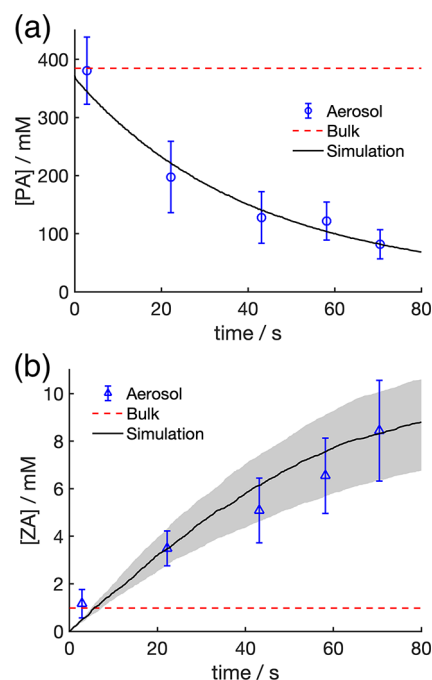


Figure 2. Kinetics of (a) $[\text{PA}]$ and (b) $[\text{ZA}]$ in aerosols versus residence time in flow tubes ($[\text{PA}]_0 = 370 \text{ mM}$). Every MS measurement is repeated three times, and the error bars represent one standard deviation. Dashed red lines are the kinetics of $[\text{PA}]$ and $[\text{ZA}]$ in a bulk solution. Black solid lines represent simulated results from the kinetic modeling discussed later. The gray shaded area in (b) shows $\sim 20\%$ margin of error for the rate constant of ZA formation ($k_{\text{rxn}} = (0.9 \pm 0.2) \times 10^{-3} \text{ M}^{-1} \text{ s}^{-1}$).

composition as aerosols (i.e., $[\text{PA}]_0 = 370 \text{ mM}$ and $[\text{NaCl}] = 4.6 \text{ M}$) (Figure S5). After 2.5 h, the MS of the bulk solution does not show significant changes in $[\text{PA}]$ and $[\text{ZA}]$, and the linear fits to the bulk data are shown for comparison as dashed lines in Figure 2a,b. The result from this control experiment agrees with previous literature where the time scale of ZA formation in bulk solutions ranges from weeks to months.^{28,29} These observations clearly demonstrate that the formation of ZA is favored in $r_{\text{avg}} = 240 \text{ nm}$ aerosol droplets, likely because the 1 nm thick air–water interface is a substantial fraction (1.25%) of the reaction environment compared to, e.g., $10^{-5}\%$ for 10 mL solution in a 50 mL sized beaker.^{27,30}

Additionally, since the formation of ZA from two PA molecules requires the elimination of water, the role of rapid water evaporation during the initial equilibration process (i.e.,

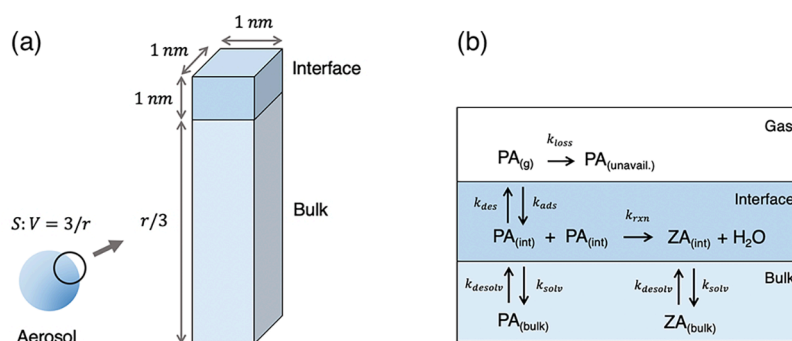
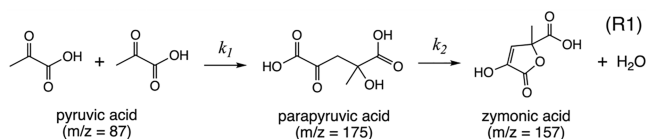


Figure 3. Graphical illustration of the model used for simulating reaction kinetics in submicron aerosols. (a) A spherical geometry of aerosols is reduced to a box model in stochastic simulation. Volumes of the interface and bulk compartments are defined as $1 \times 1 \times 1 \text{ nm}^3$ and $1 \times 1 \times r/3 \text{ nm}^3$, respectively, retaining the surface-to-volume ratio of a sphere ($3/r$). (b) Mechanism of the bulk–interface and interface–gas partitioning of PA as well as the condensation reaction at the interface of aerosols.

as the droplets exit the atomizer) to 80% RH is evaluated. As a control experiment, aerosols are generated from the solutions with the PA and NaCl concentrations identical with the equilibrated conditions at RH = 80% ($[\text{PA}] = 370 \text{ mM}$ and $[\text{NaCl}] = 4.6 \text{ M}$); thus, aerosols experience no rapid evaporation. The aerosols are then routed through the same set of flow tubes with $\sim 70 \text{ s}$ reaction time as done for the data shown in Figure 2. The results still show the formation of ZA with increasing reaction time, indicating that rapid initial water evaporation is not required to form ZA (Figure S6). It is also confirmed that the hydrolysis of ZA back into 2 pyruvic acid molecules is negligible under our conditions by running aerosols with ZA only ($[\text{ZA}]_0 = 41 \text{ mM}$) in the flow tubes (Figure S7). We find no noticeable changes in $[\text{ZA}]$ or the formation of PA with reaction time for aerosols or in bulk solutions over 2 h. This result suggests that the reverse reaction rate of the ZA formation is negligible compared to that of the forward reaction.

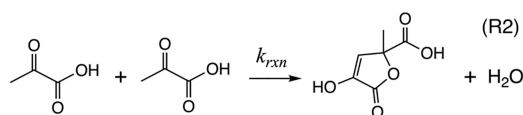
In addition to PA ($m/z = 87$) and ZA ($m/z = 157$), the kinetics of the smaller peaks ($m/z = 105, 113, 175$, and 193) in the MS spectra (Figure 1b) are shown in Figure S8. The ZA fragment peak at $m/z = 113$ ($\text{ZA-CO}_2\text{-H}^-$; identified by CID data, see Figure S2) increases as a function of time similar to the main ZA peak ($m/z = 157$). The $m/z = 105$ peak, corresponding to the hydrated diol of pyruvic acid, 2,2-dihydroxypropanoic acid (2,2-DHPA),^{26,44} exhibits decay kinetics similar to PA. Interestingly, the $m/z = 175$ peak, assigned to parapyruvic acid,^{26,43,45} also shows a steady decrease with reaction time, which warrants further discussion.

Parapyruvic acid (PPA) has been proposed as a reaction intermediate during the formation of ZA as shown in reaction R1 where both steps are acid-catalyzed.²⁷



However, in the time scale of our experiments, no significant buildup of PPA as an intermediate in aerosols is observed (Figure S8). This suggests that any PPA formed is rapidly lost to the reaction, meaning the unimolecular ring formation step (k_2) would be relatively fast, and the first bimolecular reaction (k_1) is likely the rate-determining step. Thus, we can simplify the proposed mechanism (R1) to (R2), where ZA is directly

formed from the bimolecular condensation of PA with a second-order rate constant, k_{rxn} .



As observed in Figure 2, the disappearance of PA and the formation of ZA occur simultaneously in the aerosol environment. This likely occurs at the air–water interface, which is consistent with the observations from other studies.^{24,30} Interestingly, the measured kinetic data suggest that the major contribution to the decrease in $[\text{PA}]$ over time is interfacial desorption. In the case of $[\text{PA}]_0 = 370 \text{ mM}$ aerosols, for example, the $[\text{PA}]$ is reduced to 80 mM after 70 s (Figure 2a), whereas the $[\text{ZA}]$ that is formed is only $\sim 8 \text{ mM}$ (Figure 2b). Therefore, out of 290 mM $[\text{PA}]$, only 16 mM $[\text{PA}]$ is consumed in the formation of ZA, whereas the remaining 274 mM $[\text{PA}]$ is lost due to desorption. To unravel the competition between reaction and desorption at the aerosol interface and further quantify the rate constants for each process, a kinetic model is developed.

A two-compartment model representing the interface and bulk of an aerosol droplet and a mechanistic description of the bulk–interface partitioning, adsorption–desorption, and reaction kinetics of PA and ZA is shown in Figure 3.^{11,34–39} Since the aerosols remain in the liquid phase throughout the experimental condition at 80% RH,⁴⁶ it is reasonable to assume they have a spherical geometry with surface-to-volume ratio ($S:V$) of $3/r$, where r is the volume-averaged radius of the polydisperse aerosols (240 nm, Figure S1). A box model with an interface and bulk compartments (Figure 3a) is used to set the stage for stochastic simulation of the reaction and partitioning of the species in the aerosols. The interface compartment is defined as 1 nm thick with a 1 nm^2 base area. The 1 nm interfacial thickness is consistent with the molecular dynamics (MD) simulation studies of water interfaces.^{38,47,48} The bulk compartment has a 1 nm^2 base area with a $3/r$ height to reflect the $S:V$ ratio of a sphere in the box model. We use KineticScope, a stochastic reaction–diffusion simulator, to model the kinetics of PA and ZA.^{49,50} Detailed settings and values of the input parameters for the simulations are listed in Table S1.

Figure 3b shows the elementary kinetic steps that describe (1) interface–bulk partitioning of PA and ZA, (2) desorption and adsorption of PA between interface and gas phase, and (3)

formation of ZA at the interface by condensation of two PA molecules. Although PA and ZA can exist in different forms in aqueous solution,^{28,51} for simplicity only the keto form of PA and closed enol form of ZA are considered in interfacial reactions as done in other studies.^{30,43} The interface–bulk partitioning or surface activity of PA is described by solvation (k_{solv} , interface to bulk) and desolvation (k_{desolv} , bulk to interface) rate constants. To quantify the concentration of PA at the interface ($[\text{PA}]_{\text{int}}$) available for desorption and reaction, the value of the equilibrium partitioning constant ($K_{\text{eq}}^{\text{PA}} = k_{\text{desolv}}/k_{\text{solv}}$ in units of M^{-1}) is needed. The value of $K_{\text{eq}}^{\text{PA}}$ can be obtained by fitting the Langmuir–Szyszkowski adsorption model to the experimentally measured surface tension of an aqueous PA solution.⁴³

The Langmuir–Szyszkowski equation of state (EOS) is

$$\gamma - \gamma_{\text{water}} = \Gamma_{\infty}^{\text{PA}} RT \ln(1 - \theta) \quad (1)$$

where γ is the surface tension of PA solution (N m^{-1}), γ_{water} is the surface tension of water ($72 \times 10^{-3} \text{ N m}^{-1}$),⁵² $\Gamma_{\infty}^{\text{PA}}$ is the maximum surface concentration of PA ($4.3 \times 10^{-10} \text{ mol cm}^{-2}$),⁵³ R is the gas constant, and T is the temperature (298 K). From the Langmuir equation, the fractional occupancy of PA at the interface (θ) and $K_{\text{eq}}^{\text{solv}}$ is

$$\theta = \frac{K_{\text{eq}}^{\text{solv}} [\text{PA}]_{\text{bulk}}}{1 + K_{\text{eq}}^{\text{solv}} [\text{PA}]_{\text{bulk}}} \quad (2)$$

The value $K_{\text{eq}}^{\text{PA}} = 28.5 \pm 5 \text{ M}^{-1}$ is obtained by fitting eq 1 to the surface tension data of aqueous PA solutions (Figure S9).⁴³ For partitioning of ZA, Gordon et al.⁴³ reported that PA and ZA have a similar surface propensity in MD simulations; thus, we assume an identical value of $K_{\text{eq}}^{\text{ZA}} = 28.5 \text{ M}^{-1}$. From $K_{\text{eq}}^{\text{PA}}$ values of k_{solv} and k_{desolv} for PA and ZA are defined as 100 s^{-1} and $2850 \text{ M}^{-1} \text{ s}^{-1}$, respectively, and the exact value has minimal impact on simulated results (Figure S10). A value of $k_{\text{solv}} = 100 \text{ s}^{-1}$ is consistent with solvation kinetics of similar-sized organic acids measured by Bleyers and Joos, and k_{desolv} is calculated from $k_{\text{desolv}} = K_{\text{eq}}^{\text{solv}} k_{\text{solv}}$.⁵³ Finally, $\Gamma_{\infty}^{\text{PA}}$ ($4.3 \times 10^{-10} \text{ mol cm}^{-2}$) is converted into a maximum volumetric concentration of PA at the interface ($[\text{PA}]_{\text{int}}^{\text{max}}$, unit: M) by

$$[\text{PA}]_{\text{int}}^{\text{max}} = \frac{\Gamma_{\infty}^{\text{PA}}}{\delta} \theta \approx 4.3 \text{ M} \quad (3)$$

where δ is the interfacial thickness defined as 1 nm, as discussed before (Figure 3a). The value of 4.3 M can also be interpreted as a concentration of available adsorption sites at the interface, where PA and ZA molecules occupy one and two sites, respectively. The exact values of k_{solv} , k_{desolv} , and $[\text{PA}]_{\text{int}}^{\text{max}}$ derived here are used in the simulation to reproduce the bulk–interface partitioning behavior of PA and ZA (Figure 3b).

The desorption rate of PA in aqueous aerosols is described by the Hertz–Knudsen equation^{54,55}

$$J = \frac{\alpha p_{\text{vap}}}{\sqrt{2\pi m k_{\text{B}} T}} \quad (4)$$

where J is molecular flux (units: molecules $\text{m}^{-2} \text{ s}^{-1}$), p_{vap} is the saturation vapor pressure of PA (175 Pa), α is the evaporation (desorption) coefficient (assumed as 1), m is the mass of a PA molecule ($1.46 \times 10^{-25} \text{ kg}$), and k_{B} is the Boltzmann constant. The $[\text{PA}]$ in the aerosol is relatively dilute (i.e., mM) so the Henry's law constant can be used to substitute p_{vap} :

$$\frac{J}{[\text{PA}]} = \frac{1/H_{\text{PA}}}{\sqrt{2\pi m k_{\text{B}} T}} \quad (5)$$

From prior literature, H_{PA} for PA is $3.1 \text{ mol kg}^{-1} \text{ Pa}^{-1}$.^{32,33,42} Note that the units of the left side of the equation are m s^{-1} . To obtain the desorption rate constant in units of s^{-1} , the geometry of the simulation (i.e., S/V ratio) is needed to account for surface availability for desorption. Finally, k_{des} is expressed as

$$k_{\text{des}} = \frac{A_{\text{sim}}}{V_{\text{sim}}} \frac{1/H_{\text{PA}}}{\sqrt{2\pi m k_{\text{B}} T}} \quad (6)$$

where A_{sim} and V_{sim} are the surface area and volume of the simulation geometry, respectively, as shown in Figure 3a. Equation 6 yields $k_{\text{des}} = 110 \text{ s}^{-1}$ for $r = 240 \text{ nm}$ aerosols. The rate constant for gas phase to interface adsorption (k_{ads}) can be computed in a similar manner, using the Henry's law constant. In a fully enclosed system at equilibrium, $k_{\text{ads}} = k_{\text{des}}$. Although the flow tube reactors are fully enclosed, the $[\text{PA}]$ concentration is observed to decrease over time (Figure 2a). This decrease in $[\text{PA}]$ cannot be fully explained by reactive loss, as discussed above, suggesting that PA is also lost to the reactor walls. Wall loss of gas phase molecules or aerosols are commonly observed and quantified in experimental studies utilizing flow tubes or reaction chambers.^{56,57} In the kinetic model, a rate constant for the wall loss (k_{loss}) is included as an adjustable parameter. A value of $k_{\text{loss}} = 0.1 \text{ s}^{-1}$ best replicates the measured kinetics of $[\text{PA}]$ at three different initial PA concentrations as shown in Figure 2a and Figure S4.

Lastly, the rate constant of ZA formation is described in the model as k_{rxn} . As discussed previously, this reaction is assumed to follow bimolecular reaction kinetics so the units of k_{rxn} are $\text{M}^{-1} \text{ s}^{-1}$. Additionally, we assume the condensation reaction occurs exclusively at the interface, as shown in Figure 3b, as a negligible quantity of ZA is formed in bulk PA solutions (Figure 2a and Figure S4). Therefore, k_{rxn} remains as the only unknown parameter for simulating ZA formation kinetics since the bulk–interface partitioning and desorption of PA and ZA are constrained by $K_{\text{eq}}^{\text{PA}}$, $K_{\text{eq}}^{\text{ZA}}$, and $[\text{PA}]_{\text{int}}^{\text{max}}$. A value of $k_{\text{rxn}} = (0.9 \pm 0.2) \times 10^{-3} \text{ M}^{-1} \text{ s}^{-1}$ best replicates the entire experimental data set as shown in Figure 2b and Figure S4. Although there is some evidence that the pK_{a} of carboxylic acids is altered at the air–water interface, we assume that the majority of PA at the surface is protonated, given the relatively high interfacial concentration of PA ($[\text{PA}]_{\text{int}}^{\text{max}} \sim 4.3 \text{ M}$ and $\text{pK}_{\text{a}} = 2.5$).^{58–61}

In addition to reproducing MS data, the simulated results can be used to evaluate the contributions from bulk and interface regions to the overall observed kinetics. For example, Figure 4 shows the interplay between the interface and bulk by separating the kinetics of $[\text{PA}]$ and $[\text{ZA}]$ in each compartment for the $[\text{PA}]_0 = 370 \text{ mM}$ data set (see Figure S10 for $[\text{PA}]_0 = 90$ and 230 mM aerosols). At the start of the simulation ($\sim 0 \text{ s}$), rapid partitioning of PA from the bulk to the interface is observed (Figure 4a). This partitioning leads to the depletion of $[\text{PA}]_{\text{bulk}}$, which is more significant as $[\text{PA}]_0$ decreases (Figure S11). It can also be seen in Figure 4a that the consumption rate of $[\text{PA}]$ is more significant in the bulk compartment compared to the interface, which can be explained by desorption. Because of the surface activity of PA ($K_{\text{eq}}^{\text{PA}} = 28.5 \text{ M}^{-1}$), each time a PA molecule desorbs from the interface to the gas phase, the adsorption site is quickly replaced by another PA from the bulk.

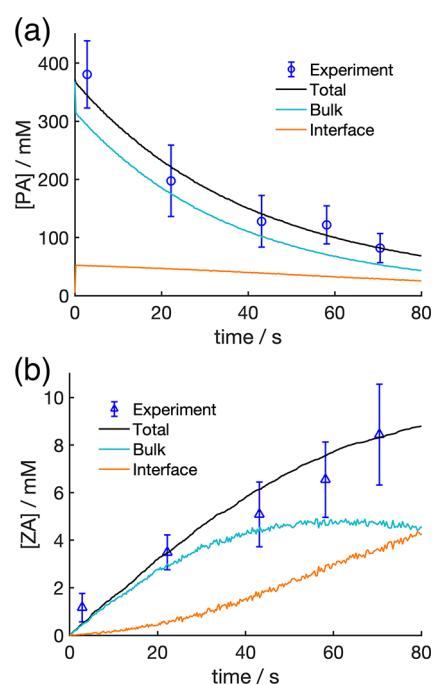


Figure 4. Detailed simulated results depicting the interface and bulk contributions to the (a) [PA] and (b) [ZA] kinetics in $[PA]_0 = 370$ mM aerosols. Blue circles represent the MS-measured concentrations. Error bars are standard deviations of three measurements. Solid black lines are simulated total concentrations of PA and ZA in aerosols, as shown in Figure 2a. Teal and orange lines are contributions from the bulk and the interface compartments, respectively

Unlike the overall decrease of PA in each compartment, the formation kinetics of ZA exhibit unique behavior. Figure 4b shows that ZA molecules predominantly partition to the bulk compartment during the early stages of the reaction (up to ~ 40 s) although the formation of ZA is restricted to the interface. Even though the surface propensities of ZA and PA are assumed to be identical, the abundance of PA and the limited number of available sites at the interface lead to the majority of ZA molecules formed at the interface to partition into bulk. However, after ~ 60 s, the ZA contribution from the bulk decreases while the coverage of ZA at the interface steadily increases. This trend is due to the decrease of PA molecules at the interface, which are consumed by ZA formation, desorption, and wall loss leaving more sites at the interface for ZA, thus increasing its bulk to interface partitioning.

Although the apparent rate constant of dark ZA formation in aerosols is obtained in this study, the rate constant for ZA formation in bulk solutions has not been reported, to our knowledge. Only the time scale of acid-catalyzed ZA formation is reported by Düwel et al., which is 20–30 days in highly acidic solutions (1 M HCl, pH ~ 0).²⁹ From these observations, one can roughly estimate the value of the rate constant in bulk solutions to be $k_{rxn,bulk} \sim 4.0 \times 10^{-8} \text{ M}^{-1} \text{ s}^{-1}$ (see Figure S12). This estimate assumes a 40% yield of ZA after 30 days as reported.²⁹ Using this value in the simulations of $[PA]_0 = 370$ mM aerosols would result in 1.1 μM of ZA formation after 100 s of reaction time as shown in Figure S11, which cannot explain the observed ~ 10 mM of [ZA] in Figure 2b.

We would note that enhanced interfacial acidity relative to the bulk can impact reaction rates, although there remains

some uncertainties about the exact value of the pH at air–water interfaces.^{62–66} Although, taking the surface activity of PA into account, the interfacial pH is likely different from that of the bulk. According to kinetic simulation, at $t = 0$, the $[PA]_0$ at the interface is ~ 4.3 M whereas the bulk $[PA]_0 \sim 300$ mM (Figure 4). Given that the bulk pK_a of PA is 2.5, the acidity of the interface is estimated to be lower by 0.5 (interfacial pH ~ 1 and bulk pH ~ 1.5). However, the slow reaction rate of PA in the bulk even in pH ~ 0 conditions ($k_{rxn,bulk} \sim 4.0 \times 10^{-8} \text{ M}^{-1} \text{ s}^{-1}$) suggests that the enhanced acidity at the interface is not the sole cause for the observed reaction enhancement. Rather, our model suggests that the accelerated formation of ZA observed in nanodroplets is due both to a larger rate coefficient (factor of $\sim 10^4$ – 10^5) and the enrichment of PA at the interface (factor of ~ 10).⁴³ It is worth noting that the value of k_{rxn} derived in this study is ~ 2 orders of magnitude smaller than the value obtained from the kinetic modeling of sessile microdroplets. This difference may originate from the differences in experimental conditions that include micron-sized sessile droplets vs submicron aerosols, [PA], [NaCl], and droplet pH.³¹

There are a number of condensation reactions, such as peptide bond formation and imine formation, which are also shown to be enhanced at the interface, possibly due to partial solvation and transition state stabilization.^{5,12,16,17} For example, the enhanced rate of imine synthesis at the interface of microdroplets investigated by Fallah-Araghi et al. and our group is on the order of 10^{-4} – $10^{-3} \text{ M}^{-1} \text{ s}^{-1}$,^{5,11} similar to the apparent value obtained for ZA formation in this study ($k_{rxn} = (0.9 \pm 0.2) \times 10^{-3} \text{ M}^{-1} \text{ s}^{-1}$). In addition, the ZA production via photochemical reactions of PA is also significantly enhanced at the interface compared to bulk, according to the study by Kappes et al.²⁶ These findings, along with our analysis, strongly suggest that the formation of ZA in aerosols is another example of a water-eliminating reaction preferentially occurring at the liquid interface.

Moreover, the enhanced concentration of surface-active reactants at the interface is considered one of the key factors of accelerated reaction kinetics in small systems.^{11,15,67} To examine the role of bulk to interface partitioning of PA (i.e., K_{eq}^{PA}) on the formation of ZA and loss of PA in aerosols, simulated kinetics with varying K_{eq}^{PA} and k_{rxn} are shown in Figure 5. The magnitude of K_{eq}^{PA} has a substantial impact on the simulated kinetics of [PA] and [ZA] as both the desorption of PA (Figure 5a) and the formation of ZA (Figure 5b) at the interface are suppressed when K_{eq}^{PA} is decreased. This tendency clearly shows that the surface activity of PA in aqueous systems is one of the underlying causes for accelerated formation of ZA. The effect of surface activity of PA on reaction acceleration is especially pronounced in this study because PA concentrations in the bulk compartment stay relatively low compared to the interface ($[PA]_{bulk} < 400$ mM vs $[PA]_{interface} = 4.3$ M), and the reactions occur exclusively at the interface.

In conclusion, the accelerated formation of ZA via the PA condensation reaction in aerosols is measured by time-resolved MS analysis. To explain the observed decrease of [PA] and increase of [ZA] in aerosols, a kinetic model, including droplet geometry, bulk to interface partitioning, interfacial reaction, and desorption, is developed. By fitting the kinetic simulation to the experimental data, the rate constant for the formation of ZA at the interface of aqueous aerosols ($k_{rxn} = (0.9 \pm 0.2) \times 10^{-3} \text{ M}^{-1} \text{ s}^{-1}$) is obtained and is estimated to be ~ 4 orders of magnitude larger than the reaction rate in bulk solutions.

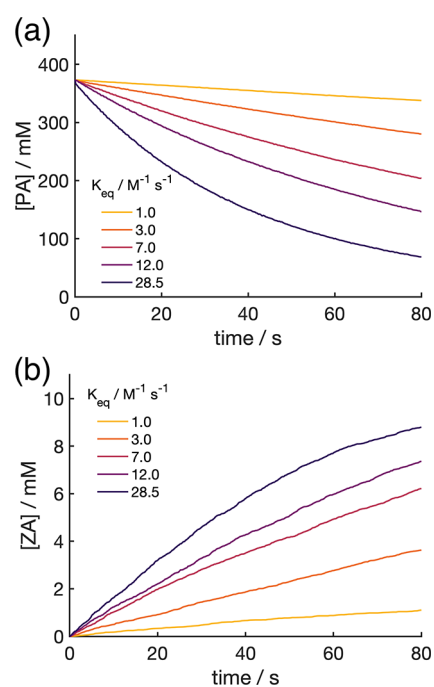


Figure 5. Simulated kinetics of (a) [PA] and (b) [ZA] assuming different values for the bulk to interface equilibrium constant of PA (K_{eq}^{PA}) from 1 to 28.5 M^{-1} while the rate of ZA formation remains constant ($k_{rxn} = 0.9 \times 10^{-3} M^{-1} s^{-1}$). The decrease of [PA] and the increase of [ZA] are significantly slower with lower K_{eq}^{PA} values, indicating that the surface activity of PA is crucial for ZA formation in aerosols

Simulated results reveal that the bulk to interface partitioning of PA and interface-enhanced condensation reaction lead to the observed accelerated ZA formation in nanodroplets. With regard to the inherent reaction acceleration of PA at the liquid interface, there is an important lingering question: what drives the reaction rate constant at the interface to be significantly higher than that in the one in bulk? Although the exact reason for the enhancement is elusive, there are possible explanations based on nontrivial physical properties at the interface including electrostatic potential fluctuation, molecular orientation, surface acidity, and partial solvation.^{12,15,68,69} Future studies about the detailed mechanism of dark PA condensation and the energetics of the enhanced chemical reaction at the liquid–air interface will greatly benefit the current understanding of the unique reactions in microcompartments currently under debate. Moreover, surface-sensitive techniques such as X-ray photoelectron spectroscopy^{70,71} and vibrational sum-frequency generation spectroscopy⁷² could be used to directly compare reaction kinetics in liquid interface versus bulk as well as the altered protonation states at the interface.^{73–75}

■ ASSOCIATED CONTENT

Supporting Information

The Supporting Information is available free of charge at <https://pubs.acs.org/doi/10.1021/acs.jpcllett.4c02736>.

Data of aerosol size, CID-MS spectra of ZA, calibration curves for MS, bulk control experiments, fitting the Langmuir equation to surface tension of PA, estimated ZA formation rate in bulk, molality (m) to molarity (M)

conversion for PA, and tabulated simulation parameters and rate constants (PDF)

■ AUTHOR INFORMATION

Corresponding Author

Kevin R. Wilson – Chemical Sciences Division, Lawrence Berkeley National Laboratory, Berkeley, California 94720, United States; orcid.org/0000-0003-0264-0872; Email: krwilson@lbl.gov

Authors

Pyeongun Kim – Chemical Sciences Division, Lawrence Berkeley National Laboratory, Berkeley, California 94720, United States; orcid.org/0000-0002-4718-4770

Ryan S. Reynolds – Chemical Sciences Division, Lawrence Berkeley National Laboratory, Berkeley, California 94720, United States; Department of Chemistry, University of California, Berkeley, Berkeley, California 94720, United States; orcid.org/0000-0002-6513-6377

Alexandra M. Deal – Chemical Sciences Division, Lawrence Berkeley National Laboratory, Berkeley, California 94720, United States

Veronica Vaida – Department of Chemistry and CIRES, University of Colorado, Boulder, Colorado 80309, United States; orcid.org/0000-0001-5863-8056

Musahid Ahmed – Chemical Sciences Division, Lawrence Berkeley National Laboratory, Berkeley, California 94720, United States; orcid.org/0000-0003-1216-673X

Complete contact information is available at:

<https://pubs.acs.org/doi/10.1021/acs.jpcllett.4c02736>

Notes

The authors declare no competing financial interest.

■ ACKNOWLEDGMENTS

The authors gratefully acknowledge support from the Director, Office of Energy Research, Office of Basic Energy Sciences, Chemical Sciences Division of the U.S. Department of Energy, under Contract No. DE-AC02-05CH11231. The Condensed Phase and Interfacial Molecular Sciences Program supported the model development, and the Gas Phase Chemical Physics program supported the Atmospheric Pressure Chemical Ionization measurements.

■ REFERENCES

- (1) Eiselthal, K. B. *Liquid Interfaces*. *Acc. Chem. Res.* **1993**, *26* (12), 636–643.
- (2) Jungwirth, P.; Tobias, D. J. *Molecular Structure of Salt Solutions: A New View of the Interface with Implications for Heterogeneous Atmospheric Chemistry*. *J. Phys. Chem. B* **2001**, *105* (43), 10468–10472.
- (3) Ni, L.; Yu, C.; Wei, Q.; Liu, D.; Qiu, J. *Pickering Emulsion Catalysis: Interfacial Chemistry, Catalyst Design, Challenges, and Perspectives*. *Angew. Chem.* **2022**, *134* (30), No. e202115885.
- (4) George, I. J.; Abbatt, J. P. D. *Heterogeneous Oxidation of Atmospheric Aerosol Particles by Gas-Phase Radicals*. *Nature Chem.* **2010**, *2* (9), 713–722.
- (5) Fallah-Araghi, A.; Meguellati, K.; Baret, J.-C.; Harrak, A. E.; Mangeat, T.; Karplus, M.; Ladame, S.; Marques, C. M.; Griffiths, A. D. *Enhanced Chemical Synthesis at Soft Interfaces: A Universal Reaction-Adsorption Mechanism in Microcompartments*. *Phys. Rev. Lett.* **2014**, *112* (2), No. 028301.

- (6) Jordan, C. J. C.; Lowe, E. A.; Verlet, J. R. R. Photooxidation of the Phenolate Anion Is Accelerated at the Water/Air Interface. *J. Am. Chem. Soc.* **2022**, *144* (31), 14012–14015.
- (7) Tian, Y.-M.; Silva, W.; Gschwind, R. M.; König, B. Accelerated Photochemical Reactions at Oil-Water Interface Exploiting Melting Point Depression. *Science* **2024**, *383* (6684), 750–756.
- (8) Gong, C.; Yuan, X.; Xing, D.; Zhang, D.; Martins-Costa, M. T. C.; Anglada, J. M.; Ruiz-López, M. F.; Francisco, J. S.; Zhang, X. Fast Sulfate Formation Initiated by the Spin-Forbidden Excitation of SO₂ at the Air–Water Interface. *J. Am. Chem. Soc.* **2022**, *144* (48), 22302–22308.
- (9) Rovelli, G.; Jacobs, M. I.; Willis, M. D.; Rapf, R. J.; Prophet, A. M.; Wilson, K. R. A Critical Analysis of Electrospray Techniques for the Determination of Accelerated Rates and Mechanisms of Chemical Reactions in Droplets. *Chem. Sci.* **2020**, *11* (48), 13026–13043.
- (10) Wei, Z.; Li, Y.; Cooks, R. G.; Yan, X. Accelerated Reaction Kinetics in Microdroplets: Overview and Recent Developments. *Annu. Rev. Phys. Chem.* **2020**, *71* (1), 31–51.
- (11) Wilson, K. R.; Prophet, A. M.; Rovelli, G.; Willis, M. D.; Rapf, R. J.; Jacobs, M. I. A Kinetic Description of How Interfaces Accelerate Reactions in Micro-Compartments. *Chem. Sci.* **2020**, *11* (32), 8533–8545.
- (12) Martins-Costa, M. T. C.; Ruiz-López, M. F. Electrostatics and Chemical Reactivity at the Air–Water Interface. *J. Am. Chem. Soc.* **2023**, *145* (2), 1400–1406.
- (13) Xia, D.; Chen, J.; Xie, H.-B.; Zhong, J.; Francisco, J. S. Counterintuitive Oxidation of Alcohols at Air–Water Interfaces. *J. Am. Chem. Soc.* **2023**, *145* (8), 4791–4799.
- (14) Wilson, K. R.; Prophet, A. M. Chemical Kinetics in Microdroplets. *Annu. Rev. Phys. Chem.* **2024**, *75*, 185–208.
- (15) Ben-Amotz, D. Interfacial Chemical Reactivity Enhancement. *J. Chem. Phys.* **2024**, *160* (8), No. 084704.
- (16) Griffith, E. C.; Vaida, V. In Situ Observation of Peptide Bond Formation at the Water–Air Interface. *Proc. Natl. Acad. Sci. U. S. A.* **2012**, *109* (39), 15697–15701.
- (17) Deal, A. M.; Rapf, R. J.; Vaida, V. Water–Air Interfaces as Environments to Address the Water Paradox in Prebiotic Chemistry: A Physical Chemistry Perspective. *J. Phys. Chem. A* **2021**, *125* (23), 4929–4942.
- (18) Andreae, M. O.; Talbot, R. W.; Li, S.-M. Atmospheric Measurements of Pyruvic and Formic Acid. *J. Geophys. Res.* **1987**, *92* (D6), 6635.
- (19) Talbot, R. W.; Andreae, M. O.; Berresheim, H.; Jacob, D. J.; Beecher, K. M. Sources and Sinks of Formic, Acetic, and Pyruvic Acids over Central Amazonia: 2. Wet Season. *J. Geophys. Res.* **1990**, *95* (D10), 16799–16811.
- (20) Eger, P. G.; Schuladen, J.; Sobanski, N.; Fischer, H.; Karu, E.; Williams, J.; Riva, M.; Zha, Q.; Ehn, M.; Quéléver, L. L. J.; Schallhart, S.; Lelieveld, J.; Crowley, J. N. Pyruvic Acid in the Boreal Forest: Gas-Phase Mixing Ratios and Impact on Radical Chemistry. *Atmospheric Chemistry and Physics* **2020**, *20* (6), 3697–3711.
- (21) Horowitz, A.; Meller, R.; Moortgat, G. K. The UV–VIS Absorption Cross Sections of the α -Dicarbonyl Compounds: Pyruvic Acid, Biacetyl and Glyoxal. *J. Photochem. Photobiol., A* **2001**, *146*, 19.
- (22) Griffith, E. C.; Carpenter, B. K.; Shoemaker, R. K.; Vaida, V. Photochemistry of Aqueous Pyruvic Acid. *Proc. Natl. Acad. Sci. U. S. A.* **2013**, *110* (29), 11714–11719.
- (23) Reed Harris, A. E.; Ervens, B.; Shoemaker, R. K.; Kroll, J. A.; Rapf, R. J.; Griffith, E. C.; Monod, A.; Vaida, V. Photochemical Kinetics of Pyruvic Acid in Aqueous Solution. *J. Phys. Chem. A* **2014**, *118* (37), 8505–8516.
- (24) Reed Harris, A. E.; Pajunoja, A.; Cazaunau, M.; Gratien, A.; Pangu, E.; Monod, A.; Griffith, E. C.; Virtanen, A.; Doussin, J.-F.; Vaida, V. Multiphase Photochemistry of Pyruvic Acid under Atmospheric Conditions. *J. Phys. Chem. A* **2017**, *121* (18), 3327–3339.
- (25) Luo, M.; Shemesh, D.; Sullivan, M. N.; Alves, M. R.; Song, M.; Gerber, R. B.; Grassian, V. H. Impact of pH and NaCl and CaCl₂ Salts on the Speciation and Photochemistry of Pyruvic Acid in the Aqueous Phase. *J. Phys. Chem. A* **2020**, *124* (25), 5071–5080.
- (26) Kappes, K. J.; Deal, A. M.; Jespersen, M. F.; Blair, S. L.; Doussin, J.-F.; Cazaunau, M.; Pangu, E.; Hopper, B. N.; Johnson, M. S.; Vaida, V. Chemistry and Photochemistry of Pyruvic Acid at the Air–Water Interface. *J. Phys. Chem. A* **2021**, *125* (4), 1036–1049.
- (27) Petters, S. S.; Hilditch, T. G.; Tomaz, S.; Miles, R. E. H.; Reid, J. P.; Turpin, B. J. Volatility Change during Droplet Evaporation of Pyruvic Acid. *ACS Earth Space Chem.* **2020**, *4* (5), 741–749.
- (28) Perkins, R. J.; Shoemaker, R. K.; Carpenter, B. K.; Vaida, V. Chemical Equilibria and Kinetics in Aqueous Solutions of Zymonic Acid. *J. Phys. Chem. A* **2016**, *120* (51), 10096–10107.
- (29) Düwel, S.; Hundshammer, C.; Gersch, M.; Feuerecker, B.; Steiger, K.; Buck, A.; Walch, A.; Haase, A.; Glaser, S. J.; Schwaiger, M.; Schilling, F. Imaging of pH in Vivo Using Hyperpolarized ¹³C-Labelled Zymonic Acid. *Nat. Commun.* **2017**, *8* (1), 15126.
- (30) Li, M.; Boothby, C.; Continetti, R. E.; Grassian, V. H. Size-Dependent Sigmoidal Reaction Kinetics for Pyruvic Acid Condensation at the Air–Water Interface in Aqueous Microdroplets. *J. Am. Chem. Soc.* **2023**, *145* (41), 22317–22321.
- (31) Li, M.; Yang, S.; Rathi, M.; Kumar, S.; Dutcher, C. S.; Grassian, V. H. Enhanced Condensation Kinetics in Aqueous Microdroplets Driven by Coupled Surface Reactions and Gas-Phase Partitioning. *Chem. Sci.* **2024**, *15* (33), 13429–13441.
- (32) Khan, I.; Brimblecombe, P. Henry's Law Constants of Low Molecular Weight (<130) Organic Acids. *J. Aerosol Sci.* **1992**, *23*, 897–900.
- (33) Khan, I.; Brimblecombe, P.; Clegg, S. L. The Henry's Law Constants of Pyruvic and Methacrylic Acids. *Environmental Technology* **1992**, *13* (6), 587–593.
- (34) Houle, F. A.; Miles, R. E. H.; Pollak, C. J.; Reid, J. P. A Purely Kinetic Description of the Evaporation of Water Droplets. *J. Chem. Phys.* **2021**, *154* (5), No. 054501.
- (35) Wilson, K. R.; Prophet, A. M.; Willis, M. D. A Kinetic Model for Predicting Trace Gas Uptake and Reaction. *J. Phys. Chem. A* **2022**, *126* (40), 7291–7308.
- (36) Willis, M. D.; Wilson, K. R. Coupled Interfacial and Bulk Kinetics Govern the Timescales of Multiphase Ozonolysis Reactions. *J. Phys. Chem. A* **2022**, *126* (30), 4991–5010.
- (37) Brown, E. K.; Rovelli, G.; Wilson, K. R. pH Jump Kinetics in Colliding Microdroplets: Accelerated Synthesis of Azamonardine from Dopamine and Resorcinol. *Chem. Sci.* **2023**, *14* (23), 6430–6442.
- (38) Prophet, A. M.; Polley, K.; Van Berkel, G. J.; Limmer, D. T.; Wilson, K. R. Iodide Oxidation by Ozone at the Surface of Aqueous Microdroplets. *Chem. Sci.* **2024**, *15* (2), 736–756.
- (39) Houle, F. A.; Hinsberg, W. D.; Wilson, K. R. Oxidation of a Model Alkane Aerosol by OH Radical: The Emergent Nature of Reactive Uptake. *Phys. Chem. Chem. Phys.* **2015**, *17* (6), 4412–4423.
- (40) Whitby, K. T.; Liu, B. Y. H. Polystyrene Aerosols—Electrical Charge and Residue Size Distribution. *Atmospheric Environment* (1967) **1968**, *2* (2), 103–116.
- (41) Wallace, B. J.; Mongeau, M. L.; Zuend, A.; Preston, T. C. Impact of pH on Gas-Particle Partitioning of Semi-Volatile Organics in Multicomponent Aerosol. *Environ. Sci. Technol.* **2023**, *57* (44), 16974–16988.
- (42) Sander, R. Compilation of Henry's Law Constants (Version 4.0) for Water as Solvent. *Atmospheric Chemistry and Physics* **2015**, *15* (8), 4399–4981.
- (43) Gordon, B. P.; Moore, F. G.; Scatena, L. F.; Richmond, G. L. On the Rise: Experimental and Computational Vibrational Sum Frequency Spectroscopy Studies of Pyruvic Acid and Its Surface-Active Oligomer Species at the Air–Water Interface. *J. Phys. Chem. A* **2019**, *123* (49), 10609–10619.
- (44) Barquilla, M. D. P.; Mayes, M. L. Role of Hydrogen Bonding in Bulk Aqueous Phase Decomposition, Complexation, and Covalent Hydration of Pyruvic Acid. *Phys. Chem. Chem. Phys.* **2022**, *24* (41), 25151–25170.

- (45) Rapf, R. J.; Perkins, R. J.; Carpenter, B. K.; Vaida, V. Mechanistic Description of Photochemical Oligomer Formation from Aqueous Pyruvic Acid. *J. Phys. Chem. A* **2017**, *121* (22), 4272–4282.
- (46) Braun, C.; Krieger, U. K. Two-Dimensional Angular Light-Scattering in Aqueous NaCl Single Aerosol Particles during Deliquescence and Efflorescence. *Opt. Express* **2001**, *8* (6), 314.
- (47) Herdes, C.; Ervik, Å.; Mejía, A.; Müller, E. A. Prediction of the Water/Oil Interfacial Tension from Molecular Simulations Using the Coarse-Grained SAFT- γ Mie Force Field. *Fluid Phase Equilib.* **2018**, *476*, 9–15.
- (48) Martins-Costa, M. T. C.; Ruiz-López, M. F. Probing Solvation Electrostatics at the Air–Water Interface. *Theor. Chem. Acc.* **2023**, *142* (3), 29.
- (49) Hinsberg, W.; Houle, F. Kinetiscope: A Stochastic Kinetics Simulator. Available at hinsberg.net/kinetiscope, 2017.
- (50) Wiegel, A. A.; Wilson, K. R.; Hinsberg, W. D.; Houle, F. A. Stochastic Methods for Aerosol Chemistry: A Compact Molecular Description of Functionalization and Fragmentation in the Heterogeneous Oxidation of Squalane Aerosol by OH Radicals. *Phys. Chem. Chem. Phys.* **2015**, *17* (6), 4398–4411.
- (51) Rapf, R. J.; Dooley, M. R.; Kappes, K.; Perkins, R. J.; Vaida, V. pH Dependence of the Aqueous Photochemistry of α -Keto Acids. *J. Phys. Chem. A* **2017**, *121* (44), 8368–8379.
- (52) Vargaftik, N. B.; Volkov, B. N.; Voljak, L. D. International Tables of the Surface Tension of Water. *J. Phys. Chem. Ref. Data* **1983**, *12* (3), 817–820.
- (53) Bleys, G.; Joos, P. Adsorption Kinetics of Bolaform Surfactants at the Air/Water Interface. *J. Phys. Chem.* **1985**, *89* (6), 1027–1032.
- (54) Holyst, R.; Litniewski, M.; Jakubczyk, D. A Molecular Dynamics Test of the Hertz–Knudsen Equation for Evaporating Liquids. *Soft Matter* **2015**, *11* (36), 7201–7206.
- (55) Persad, A. H.; Ward, C. A. Expressions for the Evaporation and Condensation Coefficients in the Hertz–Knudsen Relation. *Chem. Rev.* **2016**, *116* (14), 7727–7767.
- (56) Seinfeld, J. H.; Kleindienst, T. E.; Edney, E. O.; Cohen, J. B. Aerosol Growth in a Steady-State, Continuous Flow Chamber: Application to Studies of Secondary Aerosol Formation. *Aerosol Sci. Technol.* **2003**, *37* (9), 728–734.
- (57) Che, D. L.; Smith, J. D.; Leone, S. R.; Ahmed, M.; Wilson, K. R. Quantifying the Reactive Uptake of OH by Organic Aerosols in a Continuous Flow Stirred Tank Reactor. *Phys. Chem. Chem. Phys.* **2009**, *11* (36), 7885.
- (58) Wellen, B. A.; Lach, E. A.; Allen, H. C. Surface pK_a of Octanoic, Nonanoic, and Decanoic Fatty Acids at the Air–Water Interface: Applications to Atmospheric Aerosol Chemistry. *Phys. Chem. Chem. Phys.* **2017**, *19* (39), 26551–26558.
- (59) Enami, S.; Fujii, T.; Sakamoto, Y.; Hama, T.; Kajii, Y. Carboxylate Ion Availability at the Air–Water Interface. *J. Phys. Chem. A* **2016**, *120* (46), 9224–9234.
- (60) Dawson, R. M. C.; Elliott, W. H. *Buffers and Physiological Media. Data for Biochemical Research*; Oxford University Press: Oxford, 1959; pp 200–205.
- (61) Eugene, A. J.; Pillar-Little, E. A.; Colussi, A. J.; Guzman, M. I. Enhanced Acidity of Acetic and Pyruvic Acids on the Surface of Water. *Langmuir* **2018**, *34* (31), 9307–9313.
- (62) Enami, S.; Stewart, L. A.; Hoffmann, M. R.; Colussi, A. J. Superacid Chemistry on Mildly Acidic Water. *J. Phys. Chem. Lett.* **2010**, *1* (24), 3488–3493.
- (63) Beattie, J. K.; Djerdjev, A. M.; Warr, G. G. The Surface of Neat Water Is Basic. *Faraday Discuss.* **2009**, *141*, 31–39.
- (64) Li, M.; Kan, Y.; Su, H.; Pöschl, U.; Parekh, S. H.; Bonn, M.; Cheng, Y. Spatial Homogeneity of pH in Aerosol Microdroplets. *Chem.* **2023**, *9* (4), 1036–1046.
- (65) de la Puente, M.; Laage, D. How the Acidity of Water Droplets and Films Is Controlled by the Air–Water Interface. *J. Am. Chem. Soc.* **2023**, *145* (46), 25186–25194.
- (66) Baer, M. D.; Kuo, I.-F. W.; Tobias, D. J.; Mundy, C. J. Toward a Unified Picture of the Water Self-Ions at the Air–Water Interface: A Density Functional Theory Perspective. *J. Phys. Chem. B* **2014**, *118* (28), 8364–8372.
- (67) Vannoy, K. J.; Edwards, M. Q.; Renault, C.; Dick, J. E. An Electrochemical Perspective on Reaction Acceleration in Droplets. *Annual Review of Analytical Chemistry* **2024**, *17*, 149–171.
- (68) Lesnicki, D.; Wank, V.; Cyran, J. D.; Backus, E. H. G.; Sulpizi, M. Lower Degree of Dissociation of Pyruvic Acid at Water Surfaces than in Bulk. *Phys. Chem. Chem. Phys.* **2022**, *24* (22), 13510–13513.
- (69) Kusaka, R.; Nihonyanagi, S.; Tahara, T. The Photochemical Reaction of Phenol Becomes Ultrafast at the Air–Water Interface. *Nat. Chem.* **2021**, *13* (4), 306–311.
- (70) Ahmed, M.; Lu, W. Probing Complex Chemical Processes at the Molecular Level with Vibrational Spectroscopy and X-Ray Tools. *J. Phys. Chem. Lett.* **2023**, *14* (41), 9265–9278.
- (71) Kim, P.; Weeraratna, C.; Nemšák, S.; Dias, N.; Lemmens, A. K.; Wilson, K. R.; Ahmed, M. Interfacial Nanostructure and Hydrogen Bond Networks of Choline Chloride and Glycerol Mixtures Probed with X-Ray and Vibrational Spectroscopies. *J. Phys. Chem. Lett.* **2024**, *15* (11), 3002–3010.
- (72) Saak, C.-M.; Backus, E. H. G. The Role of Sum-Frequency Generation Spectroscopy in Understanding On-Surface Reactions and Dynamics in Atmospheric Model-Systems. *J. Phys. Chem. Lett.* **2024**, *15* (17), 4546–4559.
- (73) Xu, B.; Jacobs, M. I.; Kostko, O.; Ahmed, M. Guanidinium Group Remains Protonated in a Strongly Basic Arginine Solution. *ChemPhysChem* **2017**, *18* (12), 1503–1506.
- (74) Weeraratna, C.; Tang, X.; Kostko, O.; Rapp, V. H.; Gundel, L. A.; Destailhats, H.; Ahmed, M. Fraction of Free-Base Nicotine in Simulated Vaping Aerosol Particles Determined by X-Ray Spectroscopies. *J. Phys. Chem. Lett.* **2023**, *14* (5), 1279–1287.
- (75) Kostko, O.; Xu, B.; Ahmed, M. Local Electronic Structure of Histidine in Aqueous Solution. *Phys. Chem. Chem. Phys.* **2021**, *23* (14), 8847–8853.